ACADEMIC PRESS

Available online at www.sciencedirect.com

SCIENCE DIRECT®

Journal of Sound and Vibration 264 (2003) 929–950

JOURNAL OF SOUND AND VIBRATION

www.elsevier.com/locate/jsvi

Vibrational response prediction of a pneumatic tyre using an orthotropic two-plate wave model

J.M. Muggleton*, B.R. Mace, M.J. Brennan

Institute of Sound and Vibration Research, Southampton University, Highfield, Southampton SO17 1BJ, UK

Received 19 December 2001; accepted 24 June 2002

Abstract

A wave model to predict the vibrational response of a pneumatic tyre subject to line force excitation is presented. The tread and sidewalls are each modelled as thin, flat orthotropic plates with in-plane tension, which are joined together by a translational stiffness, and to a rigid rim. The dynamic response of the tyre to harmonic excitation is decomposed into spatial harmonics around the circumference, and waves in the meridional direction. At low frequencies (<100 Hz), the response is stiffness-like, and is controlled by the sidewall properties and tension effects resulting from the tyre pressure. In the mid-frequency range (100–500 Hz), a resonant response is observed, associated with modes both across and around the tyre. At high frequencies (>500 Hz), the response tends towards that of an infinite orthotropic plate. Experiments have been conducted on an inflated tyre fitted to a wheel rim to confirm the theoretical findings. The results show reasonable agreement with the predictions, the model accurately reflecting the phenomenological behaviour.

© 2002 Elsevier Science Ltd. All rights reserved.

1. Introduction

Vehicle noise is becoming of increasing concern and tyre noise is a major contribution to this [1]. There is consequently a need to model the vibrational behaviour of the tyre, so that the resultant noise radiation can be predicted and the tyre subsequently redesigned to reduce the noise.

A number of previous studies have addressed this problem. Finite element (FE) methods have been used to predict the vibrational response of tyres, for example [2]. However, because the wavelengths of bending waves in the tread and sidewall are so short at frequencies greater than

*Corresponding author.
E-mail address: jm9@soton.ac.uk (J.M. Muggleton).

0022-460X/03/$ - see front matter © 2002 Elsevier Science Ltd. All rights reserved.
doi:10.1016/S0022-460X(02)01190-2

about 500 Hz, the size of the FE model is large, and it is prohibitively expensive to use FE methods. Tyre noise is significant at frequencies up to several kHz, and it is this which provides the motivation for alternative modelling methods and, in particular, wave methods. Kropp [3] developed a model based on a simple ring to predict the tread vibration; Pinnington and Briscoe [4] modelled the tread as an infinite, tensioned Timshenko beam on a sidewall impedance, allowing for both one-dimensional travelling waves and higher order travelling modes with an integral number of half-wavelengths across the tread. Bolton et al. [5] also suggest a decomposition of the tyre response into propagation in the circumferential direction considered together with the existence of higher order modes across the tyre. In all these works, whilst the problem is treated as two dimensional, in essence one-dimensional wave propagation is considered in the circumferential direction.

This paper provides an approach to the modelling of high-frequency tyre vibrations which differs from previous approaches. A wave model of the dynamics of a tyre is presented in which the flexural wave response is described by two-dimensional wave equations. Here, however, the primary propagation direction is considered to be across the tyre, whilst variation in the circumferential direction is accounted for by decomposing the response into harmonic components around the tyre. The method adopted to solve the equations of motion is an extension of that proposed by Mace for beams [6], in which both propagating and nearfield wave types are taken into account.

Finally, some experimental work is presented and results compared with those of the theoretical model.

2. Wave model of a tyre

2.1. The two-plate tread/sidewall system

The system is modelled as an idealization of a tyre. The tread and sidewalls are each modelled as a thin, flat orthotropic plate, with in-plane tension, which arises as a result of the internal pressure in the tyre. Tread curvature is ignored so that the tyre is effectively "unwrapped" circumferentially, and continuity of displacement and slope is applied at the ends to reflect the fact that they are, in fact, joined. This is shown in Fig. 1. The plates are assumed to vibrate in bending and in-plane motion is neglected. To represent the longitudinal stiffness of the sidewall, it is joined to the tread via a translational stiffness as shown in Fig. 2, with continuity of slope being preserved between the two tyre elements. The stiffness arises primarily from the curvature induced by the internal pressure and also from a combination of axial stretching, bending and shear deformation. This is described in more detail in Appendix A where an expression for the sidewall stiffness is derived. The sidewall is connected to the rim by a simple support, which is assumed to be rigid. In this paper, the tyre is assumed to be symmetrical about the centreline, and hence only one-half need to be modelled in detail, with the slope being zero at the tread centreline. Whilst this is a simplification, it is intended to capture many of the salient features of the dynamic behaviour of the tyre. The method can be extended straightforwardly to excitation which is not applied along the centreline, by dividing into symmetric and asymmetric parts, and treating each separately. Excitation is a constant line force applied along a short length of the centreline of the tyre. Again,

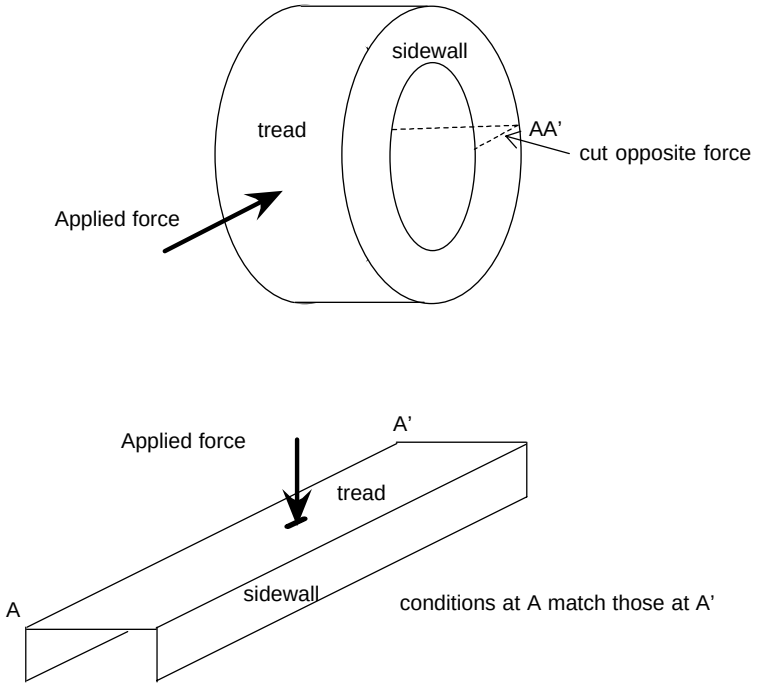

Fig. 1. Topological development of tread/sidewall tyre model.

the method can be extended to cope with excitation which is distributed across the tread; this is not so straightforward, and is the subject of current work.

A wave approach is used to model the behaviour of the system, and the dynamic response is found by summing contributions from a number of wave components. Waves are injected into the system by the force and travel through it, being reflected and transmitted at the joint between the tread and the sidewall, and again being reflected at the sidewall/rim joint. The model is developed in detail in the following sub-sections.

2.2. The equations of motion and wavenumber solutions

The transverse displacement $w(x, y, t)$ in both the tread and sidewall satisfies the plate equation [7]

$$D_{xx}\frac{\partial^4 w}{\partial x^4} + D_{yy}\frac{\partial^4 w}{\partial y^4} + 2D_3\frac{\partial^4 w}{\partial x^2 \partial y^2} - T_x\frac{\partial^2 w}{\partial x^2} - T_y\frac{\partial^2 w}{\partial y^2} = -\rho h\frac{\partial^2 w}{\partial t^2}, \tag{1}$$

where D_{xx}, D_{yy} and D_3 are the plate bending stiffnesses, T_x and T_y are the x-wise and y-wise tensions, respectively, and ρ and h are the plate density and thickness, respectively. The bending stiffnesses are given by

$$D_{xx} = E_x(1 + \mathrm{i}\eta)h^3/12(1 - \nu_{xy}\nu_{yx}), \quad D_{yy} = E_y(1 + \mathrm{i}\eta)h^3/12(1 - \nu_{xy}\nu_{yx})$$

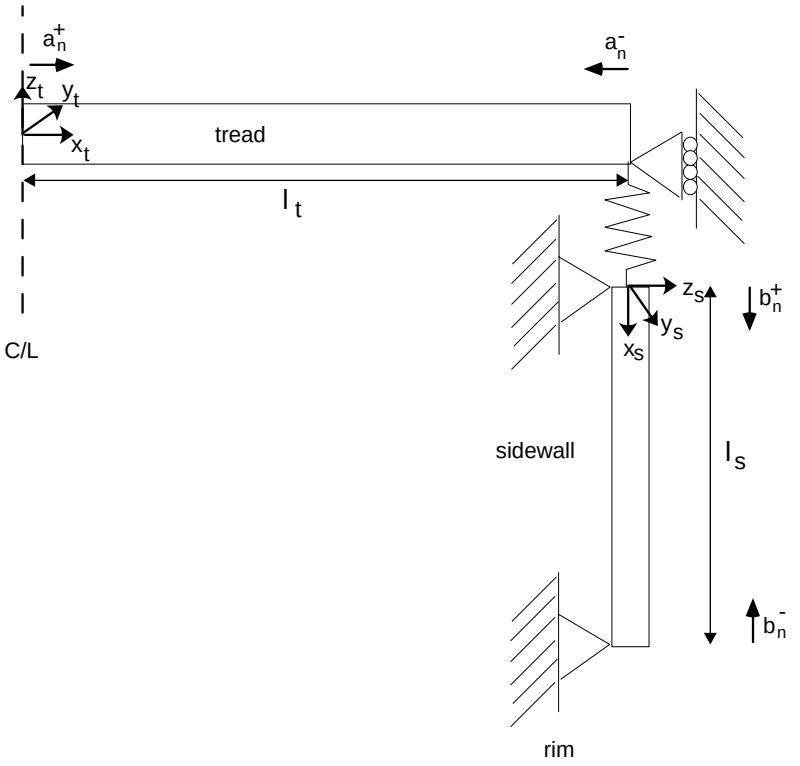

Fig. 2. Representation of section of tyre.

and

$$D_3 = D_{xy} + 2D_{66},$$

where

$$D_{xy} = v_{yx}D_x = v_{xy}D_y, \quad D_{66} = \frac{G_{xy}(1 + i\eta)h^3}{12}.$$

E_x and E_y are the elastic moduli in the x and y directions, respectively; G_{xy} is the shear modulus in the $x - y$ plane; v_{xy} and v_{yx} are the Poisson's ratios, and η is the loss factor. The material properties of the tread are, of course, different from those of the sidewall.

The internal shear forces S_x and S_y are given by

$$S_x = T_x\frac{\partial w}{\partial x} - D_{xx}\frac{\partial^3 w}{\partial x^3} - D_3\frac{\partial^3 w}{\partial x\,\partial y^2},$$

$$S_y = T_y\frac{\partial w}{\partial y} - D_{yy}\frac{\partial^3 w}{\partial y^3} - D_3\frac{\partial^3 w}{\partial x^2\partial y} \tag{2}$$

and the bending moments M_x and M_y and twisting moment M_{xy} are given by

$$M_x = -D_{xx}\frac{\partial^2 w}{\partial x^2} - D_{xy}\frac{\partial^2 w}{\partial y^2},$$

$$M_y = -D_{yy}\frac{\partial^2 w}{\partial y^2} - D_{xy}\frac{\partial^2 w}{\partial x^2},$$

$$M_{xy} = -2D_{66}\frac{\partial^2 w}{\partial x\,\partial y}. \tag{3}$$

It is assumed that the only tensions acting on each plate are T_x and T_y, and that no additional shear component exists.

All quantities are assumed to vary time harmonically at a frequency ω, and the explicit time dependence $e^{i\omega t}$ is suppressed for clarity.

Because the plates are continuous in the y direction, the response can be decomposed into spatial harmonic components in the y direction, with the nth component in this direction having a trace wavenumber k_n. This is equivalent to decomposing the response around the circumference of the tyre into a Fourier series. The displacement, $w(x,y)$, can therefore be written as

$$w(x,y) = \sum_{n=0}^{\infty} W_n(x)\cos k_n y, \tag{4}$$

where the y-component wavenumbers are

$$k_n = \frac{2n\pi}{l}, \tag{5}$$

where n is an integer and where l is the circumference of the tyre.

Eq. (4) is then substituted into Eqs. (1)–(3), and, since the trace wavenumber components are independent because the system is uniform in the y direction, each component can be analyzed independently. The total response can be found by summing over all n.

From the equation of motion, Eq. (1), it can be shown that, in the absence of applied forces, wave motion of the form

$$W_n(x) = a^+_{P,n}e^{-ik^{(1)}_{x,n}x} + a^-_{P,n}e^{ik^{(1)}_{x,n}x} + a^+_{N,n}e^{-k^{(2)}_{x,n}x} + a^-_{N,n}e^{k^{(2)}_{x,n}x} \tag{6}$$

occurs for the nth wave component in each plate, where a_n are the wave amplitudes, and the wavenumbers, $k_{x,n}$, are given by

$$k^{(1)}_{x,n} = \left(\frac{-(2D_3k_n^2 + T_x) + \sqrt{4(D_3^2 - D_{xx}D_{yy})k_n^4 + 4(D_3T_x - D_{xx}T_y)k_n^2 + (T_x^2 + 4D_{xx}\rho h\omega^2)}}{2D_{xx}}\right)^{1/2}, \tag{7}$$

$$k^{(2)}_{x,n} = \left(\frac{(2D_3k_n^2 + T_x) + \sqrt{4(D_3^2 - D_{xx}D_{yy})k_n^4 + 4(D_3T_x - D_{xx}T_y)k_n^2 + (T_x^2 + 4D_{xx}\rho h\omega^2)}}{2D_{xx}}\right)^{1/2}. \tag{8}$$

The square roots are evaluated such that $\mathrm{Im}\{k_x\} \leqslant 0$ and $\mathrm{Re}\{k_x\} \geqslant 0$ if $\mathrm{Im}\{k_x\} = 0$. The form of the x-dependence in Eq. (6) has been chosen such that both $k^{(1)}$ and $k^{(2)}$ are predominantly real in

the cases of most practical importance. The amplitudes $a^{\pm}_{N,n}$ represent evanescent or nearfield waves, while $a^{\pm}_{P,n}$ represent waves which propagate freely at high enough frequency, or low enough n.

If the plate is isotropic rather than orthotropic, such that $D_{xx} = D_{yy} = D_3 = D$, and if the in-plane tensions T_x and T_y are zero, Eqs. (7) and (8) reduce to the familiar wavenumber equations for bending of an isotropic, thin plate, namely

$$k^{(1)}_{x,n} = (k_f^2 - k_n^2)^{1/2}, \quad k^{(2)}_{x,n} = (k_f^2 + k_n^2)^{1/2}, \tag{9a, b}$$

where $k_f = \sqrt{\rho h \omega^2 / D}$ is the free bending wavenumber in the plate.

For non-zero damping, the bending stiffnesses in Eqs. (7) and (8) are complex, and consequently so, too, are the wavenumbers k_x. For small damping, $k^{(2)}_{x,n}$ is typically large and predominantly real, and therefore represents nearfield waves, significant only at and around the excitation point and plate boundaries. For high enough frequency, the wavenumber $k^{(1)}_{x,n}$ is predominantly real and represents a true wave motion which can propagate energy over significant distances. Below a particular cut-off frequency, however, $k^{(1)}_{x,n}$ becomes predominantly imaginary, and the corresponding waves become similar to nearfield waves.

2.3. The wave model

2.3.1. Wave propagation

For each circumferential order n, waves can propagate in the tread and sidewall in both positive and negative x directions. At some point in the system, the vector of positive-going wave amplitudes can be written as

$$\mathbf{a}^{+}_{n} = \begin{bmatrix} a^{+}_{P,n} \\ a^{+}_{N,n} \end{bmatrix}. \tag{10}$$

After propagation over a distance l_x, the wave amplitudes become $\mathbf{S}_n \mathbf{a}^{+}_{n}$ where

$$\mathbf{S}_n = \begin{bmatrix} e^{-ik^{(1)}_{x,n} l_x} & 0 \\ 0 & e^{-k^{(2)}_{x,n} l_x} \end{bmatrix} \tag{11}$$

is the propagation matrix for the nth trace wavenumber component. Similar expressions hold for the propagation of negative-going waves. These propagation relations can be used to relate wave amplitudes at various positions within the coupled system.

2.3.2. Wave transmission and reflection

When waves are incident at the discontinuity between the tread and sidewall plates, reflected and transmitted waves will be produced. Similarly, waves incident on the sidewall/rim joint will be reflected. With reference to Fig. 3, the wave amplitudes at a joint are related by

$$\mathbf{b}^{+}_{n} = \mathbf{T}_{ab,n} \mathbf{a}^{+}_{n} + \mathbf{R}_{bb,n} \mathbf{b}^{-}_{n}, \quad \mathbf{a}^{-}_{n} = \mathbf{R}_{aa,n} \mathbf{a}^{+}_{n} + \mathbf{T}_{ba,n} \mathbf{b}^{-}_{n}, \tag{12a, b}$$

where $\mathbf{R}_{,n}$ and $\mathbf{T}_{,n}$ are reflection and transmission matrices for the nth trace wavenumber component at the joint. Because the tread/sidewall junction is uniform, incident waves of a given trace wavenumber produce only reflected and transmitted waves with that same trace wavenumber.

The reflection and transmission matrices for the tread/sidewall junction, shown in Fig. 4a, and the sidewall/rim joint (Fig. 4b) can be found by considering continuity and equilibrium at that junction. Given the assumptions described in Section 2.1, continuity at the junction implies

$$(w_s)_0 = 0, \tag{13}$$

$$\left(\frac{\partial w_t}{\partial x_t}\right)_{l_t} = \left(\frac{\partial w_s}{\partial x_s}\right)_0, \tag{14}$$

$$K_s(w_t)_{l_t} = -(S_{x,t})_{l_t}, \tag{15}$$

$$(M_{x,t})_{l_t} = (M_{x,s})_0, \tag{16}$$

where the subscripts t and s refer to the tread and sidewall, respectively, and quantities are evaluated at the joint.

For the sidewall/rim joint shown in Fig. 4b, the boundary conditions are

$$(w_s)_{l_s} = 0, \tag{17}$$

$$(M_{x,s})_{l_s} = 0. \tag{18}$$

From these relationships, the reflection and transmission matrices can be calculated for each trace wavenumber component separately.

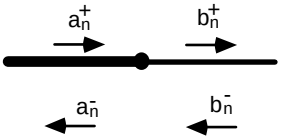

Fig. 3. Wave reflection and transmission at a joint.

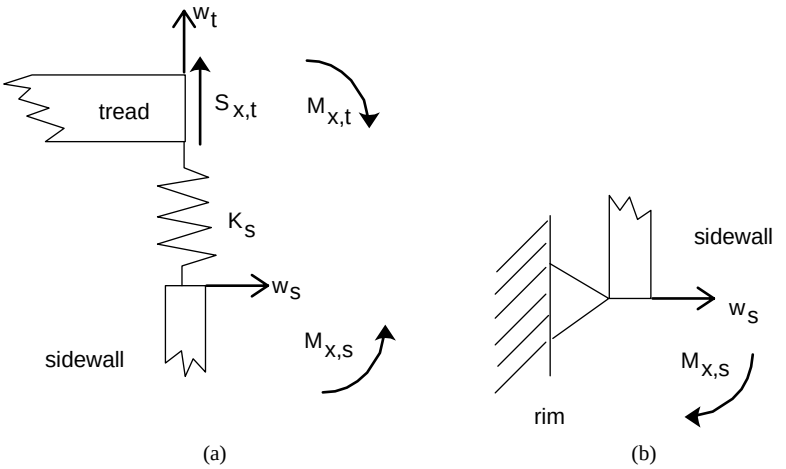

Fig. 4. Displacements, forces and moments at the joint: (a) tread/sidewall joint and (b) sidewall/rim.

2.3.3. Excitation

At the excitation point on the tread, a uniform force, Q, is applied along a length d at the tyre centreline. This force can be decomposed into harmonic components of force per unit length around the circumference of the tyre, F_n, such that

$$\frac{Q}{d} = \frac{F_0}{2} + \sum_{n=1}^{\infty} F_n \cos k_n y, \tag{19}$$

where F_n is given by

$$F_n = \frac{2}{l}\int_{-d/2}^{d/2} \frac{Q}{d} \cos k_n y \, \mathrm{d}y = \frac{2Q}{l}\frac{\sin(k_n d/2)}{(k_n d/2)}. \tag{20}$$

Waves are generated by the force, and, considering continuity and equilibrium at the excitation point, the vector of wave amplitudes generated for the nth trace wavenumber, $\mathbf{q}_n^+$ can be found.

Continuity and symmetry at the input give

$$(w_t)_{0_{RHS}} = (w_t)_{0_{LHS}}, \tag{21}$$

$$\left(\frac{\partial w_t}{\partial x}\right)_{0_{RHS}} = \left(\frac{\partial w_t}{\partial x}\right)_{0_{LHS}} = 0. \tag{22}$$

Equilibrium and symmetry at the input give

$$(S_{x,t})_{0_{RHS}} + (S_{x,t})_{0_{LHS}} = F_n, \tag{23}$$

$$(M_{x,t})_{0_{RHS}} + (M_{x,t})_{0_{LHS}} = 0. \tag{24}$$

The nth trace wavenumber, $\mathbf{q}_n^+$ is then given by

$$\mathbf{q}_n^+ = \begin{bmatrix} q_{P,n}^+ \\ q_{N,n}^+ \end{bmatrix}, \tag{25}$$

where

$$q_{P,n}^+ = \frac{\mathrm{i}F_n}{2D_{xx}k_{x,n}^{(1)}((k_{x,n}^{(1)})^2 + (k_{x,n}^{(2)})^2)} \quad \text{and} \quad q_{N,n}^+ = \frac{\mathrm{i}F_n}{2D_{xx}k_{x,n}^{(2)}((k_{x,n}^{(1)})^2 + (k_{x,n}^{(2)})^2)} \tag{26a, b}$$

2.3.4. Assembly of wave amplitude equations

Fig. 2 shows the system with vectors of positive- and negative-going wave amplitudes for the nth trace wavenumber component marked at various locations. The locations are chosen so that all waves propagate into the plates from the points at which they are defined, and hence decay as they do so. This ensures that the resulting system of matrices is well conditioned. Propagation, reflection, transmission and excitation equations can be written systematically to relate the wave

amplitudes at the various locations. In matrix form, these equations can be assembled to give

$$\begin{bmatrix} \mathbf{I} & -\mathbf{S}_{t,n} & \mathbf{0} & \mathbf{0} \\ -\mathbf{R}_{tt,n}\mathbf{S}_{t,n} & \mathbf{I} & \mathbf{0} & -\mathbf{T}_{st,n}\mathbf{S}_{s,n} \\ -\mathbf{T}_{ts,n}\mathbf{S}_{t,n} & \mathbf{0} & \mathbf{I} & -\mathbf{R}_{ss,n}\mathbf{S}_{s,n} \\ \mathbf{0} & \mathbf{0} & -\mathbf{R}_{sr,n}\mathbf{S}_{s,n} & \mathbf{I} \end{bmatrix} \begin{bmatrix} \mathbf{a}_n^+ \\ \mathbf{a}_n^- \\ \mathbf{b}_n^+ \\ \mathbf{b}_n^- \end{bmatrix} = \begin{bmatrix} \mathbf{q}_n^+ \\ \mathbf{0} \\ \mathbf{0} \\ \mathbf{0} \end{bmatrix}, \tag{27}$$

where $\mathbf{R}$ and $\mathbf{T}$ are reflection and transmission matrices at the tread/sidewall (t/s) coupling and the sidewall/rim (s/r) joint, $\mathbf{S}_t$ and $\mathbf{S}_s$ are propagation matrices for waves in the tread travelling a distance l_t, and waves in the sidewall travelling a distance l_s, respectively, and $\mathbf{I}$ and $\mathbf{0}$ are 2×2 identity and null matrices, respectively. This set of equations can be solved in a straightforward manner to determine the wave amplitudes.

Having found the various wave amplitudes, the response at any point on the tyre surface can be found by evaluating Eq. (6) for each trace wavenumber component, and then summing over all trace wavenumber components as in Eq. (4).

2.4. Numerical results

In this section, various numerical results are presented. The material and geometric properties used were estimated from raw data for each component layer of the tyre supplied by the tyre manufacturer (see Appendix B) using the method described by Hearmon [7] for determining the bending properties of sheet materials, and are shown in Table 1. The tread and sidewall in-plane tensions were calculated as a function of internal tyre pressure, as described in Appendix C. For each case presented, 150 circumferential modes were included in the calculations. The number of modes required to ensure convergence increases with increasing frequency. Including 150 modes ensured convergence to within 0.1% to above 2 kHz.

Fig. 5 shows the magnitude of the input mobility for a tyre pressurized to 2 bar. At low frequencies (below the first peak at around 80 Hz), the response is stiffness controlled. The peak at around 80 Hz is associated with a "tread bounce" motion, in which the tread moves

Table 1
Material and geometric properties of the tyre (SI units)

Quantity	Notation	Tread	Sidewall
Young's modulus	E_x	8×10^7	9×10^7
Young's modulus	E_y	3×10^7	4×10^6
The Poisson ratio	ν_{xy}	0.42	0.38
The Poisson ratio	ν_{yx}	0.36	0.32
Shear modulus	G_{xy}	6×10^6	3×10^6
Loss factor	η	0.15	0.15
x-wise length (half-length for tread)	l_t, l_s	0.1	0.08
Thickness	h	0.016	0.01
Density	ρ	1.2×10^3	1.2×10^3
Tyre circumference	l	1.9	—
Sidewall half-angle	θ	—	30
Length over which force applied	d	0.05	—

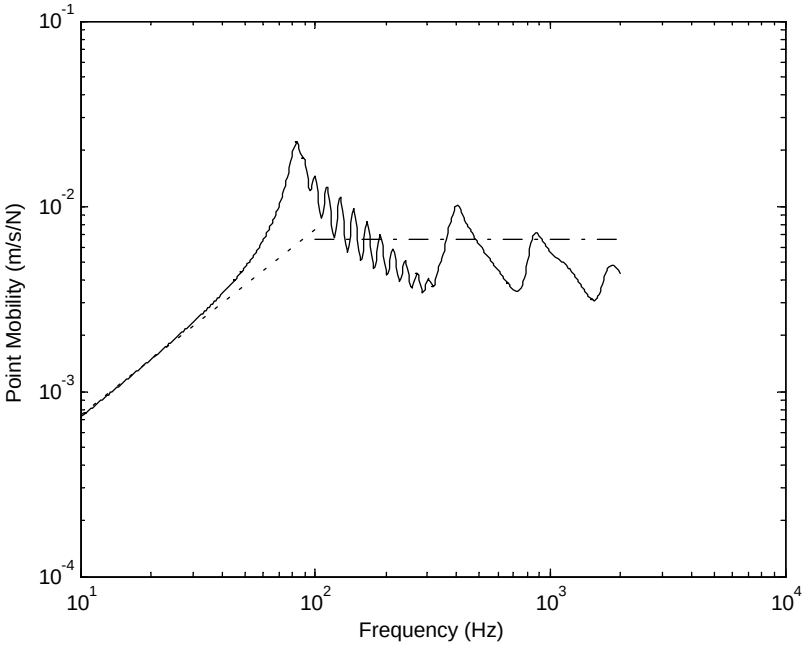

Fig. 5. Predicted input mobility at 2 bar: —— point mobility; - - - - - - stiffness line; ·-·-·-·- infinite plate response.

predominantly as a rigid mass on the sidewall spring. The group of resonances seen immediately above this first peak are associated with higher order circumferential modes with this same basic x-wise motion. At around 400 Hz, another x-wise set of modes cut on with its own group of resonances (not as clearly seen). Further groups of circumferential modes cut on at higher frequencies, most notably at around 850 Hz, and then again at just below 2 kHz. Associated with each is some characteristic x-wise motion. However, due to the high damping, individual resonance peaks cannot be clearly seen. As the frequency increases, the response first tends towards the point response of an infinite orthotropic plate whose properties equal those of the tread, the input mobility, M, being [8]

$$M = \frac{1}{8(\rho^2 h^2 D_{xx} D_{yy})^{1/4}}. \tag{28}$$

At higher frequencies still, the non-zero excitation length effectively filters out the high order circumferential modes, for which $n > l/d$, and the response falls below this value.

Fig. 6 shows the point mobility for the zeroth order ($n = 0$) circumferential mode alone, for which there is a uniform response around the circumference of the tyre. Here, the resonances correspond to the cut-on frequencies for the x-wise modes and can be more clearly seen. Fig. 7 shows the effect of reducing the excitation length, which results in the high-frequency response falling less below the infinite plate response. In general, approximately $l/2d$ (≈ 19) circumferential wave components are strongly excited, i.e., those for which the excitation length, d, is less than half the circumferential wavelength. Hence the $n = 0$ contribution is typically an order of magnitude less than the total response.

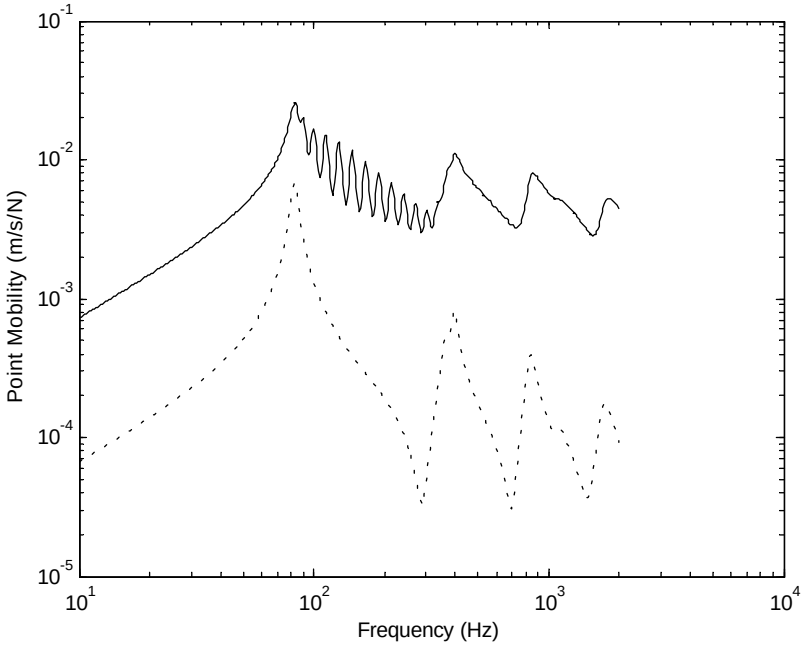

Fig. 6. Predicted response at 2 bar showing zero order circumferential mode only: —— total response; ------ zero order circumferential mode only.

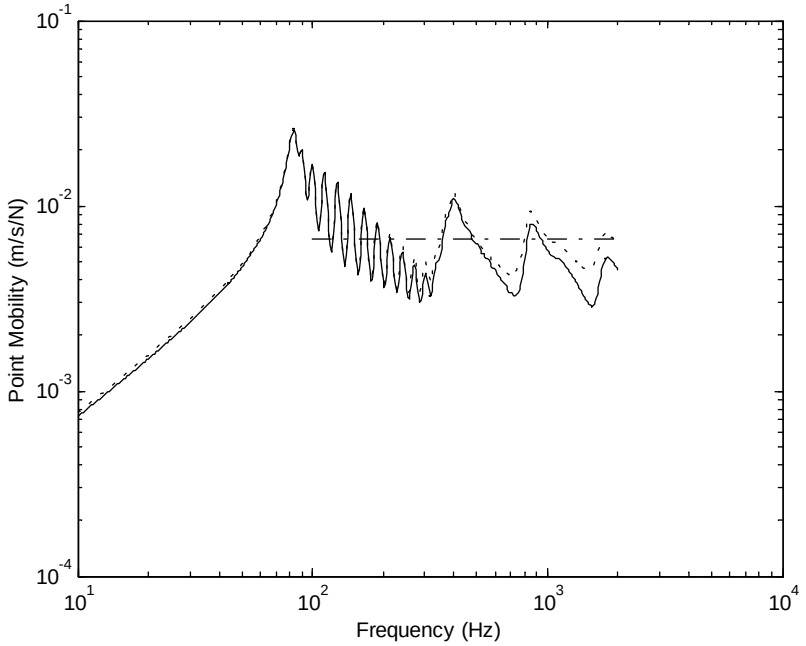

Fig. 7. Predicted response at 2 bar showing the effect of reducing the excitation length: —— 5 cm excitation length; ------ 2.5 cm excitation length; ·-·-·-·- infinite plate response.

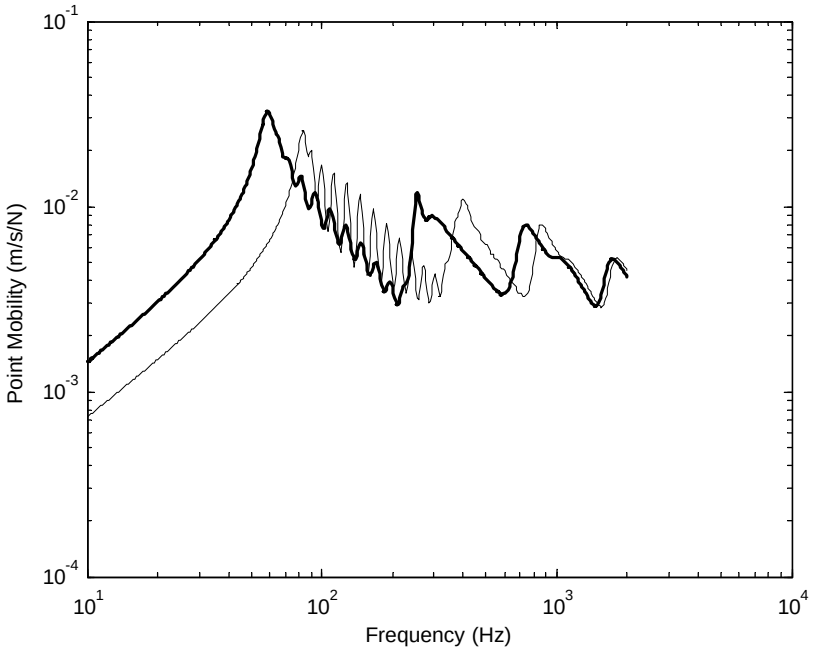

Fig. 8. Predicted response showing the effect of internal pressure: —— 0 bar; —— 2 bar.

Fig. 8 shows the two effects of reducing the internal pressure within the tyre. Firstly, the sidewall stiffness is decreased, and secondly the in-plane tensions in both the tread and sidewall are decreased. From the figure, it can be seen that decreasing the pressure increases the response at low frequencies and decreases the frequency of the first "tread bounce" resonance and of subsequent resonance peaks. The magnitudes of the resonance peaks are seen to decrease with decreasing tyre pressure, suggesting that they are controlled by in-plane tension effects in that the damping decreases as the pressure increases. However, the average magnitude of the response at these frequencies is largely unchanged. At higher frequencies, when the resonances associated with circumferential modes overlap due to the high damping, individual resonances cannot be observed and in-plane tension effects have very little influence on the overall response. In the limit, the point response of an infinite orthotropic plate under in-plane tension is independent of the tension [9].

3. Experimental work

3.1. Experimental set-up and procedure

In order to confirm the theoretical findings, some experimental measurements were made on a treadless tyre. The tyre was mounted on a steel hub which was then firmly bolted to a large frame, as shown in Fig. 9a. The tyre was excited radially by an electrodynamic shaker via a small plywood block (50 mm length × 10 mm width, which could be considered rigid within the frequency range of interest) aligned circumferentially on the centreline of the tyre. Full contact between the block and the tyre was enabled using a cement filler. The block was instrumented with

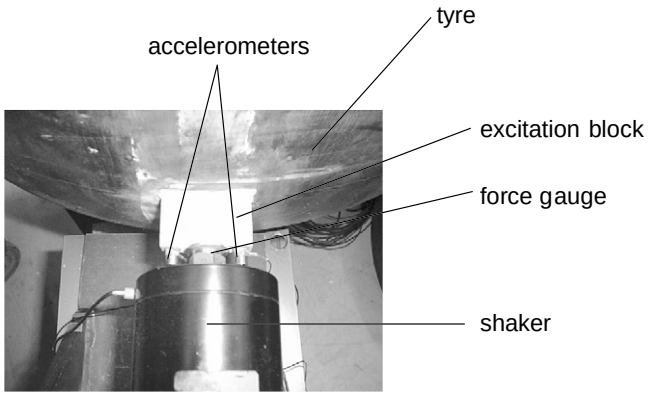

(a)

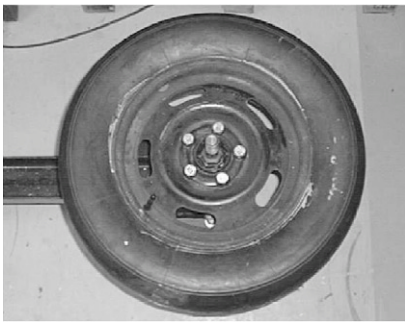

(b)

Fig. 9. Experimental arrangement: (a) shaker/instrumentation arrangement and (b)tyre mounted on frame.

a force gauge and two accelerometers, as shown in Fig. 9b. The tyre was excited with a stepped sine input from 10 Hz to 2 kHz at 2 Hz intervals, and the input mobility determined. This was calculated from the average of the two accelerometer outputs at each frequency, although differences between the accelerometer outputs were found to be minimal, indicating that the measurement block did not, in fact, rotate. In calculating the mobility, the masses of the block and instrumentation were accounted for. Measurements were made with the tyre unpressurized, and then at pressures of 1 and 2 bar. Transfer mobility measurements were also made at two locations on the tyre: on the tread at the far side of the tyre, diametrically opposite the excitation point, and midway along the sidewall, in line with the excitation point.

3.2. Results and comparison with theoretical predictions

Figs. 10a–c show the measured and predicted input mobilities at three different tyre pressures. In general, the measured and predicted data exhibit the same overall trends, with the low-frequency, stiffness-controlled region, the mid-frequency resonance groups, and the

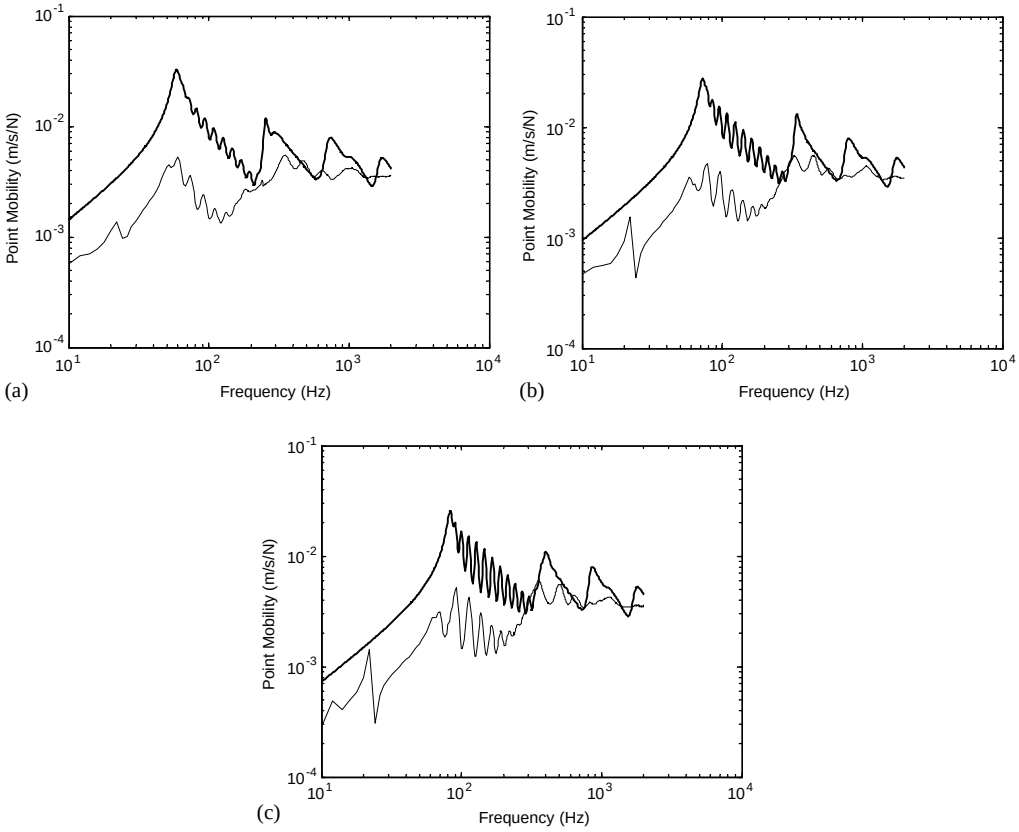

Fig. 10. Measured and predicted point response: (a) 0 bar; (b) 1 bar; (c) 2 bar; ——— predicted response; ——— measured response.

high-frequency tendency towards plate-like behaviour. In addition, the frequencies at which the various cut-on phenomena occur are well reproduced. However, the theoretical model consistently overestimates the magnitude of the response, particularly at low frequencies and for low tyre pressures. Furthermore, the circumferential resonances are slightly more closely spaced in the predictions than in the measured data, suggesting that the circumferential wavespeed has been slightly underestimated. These observations can both, in part, be attributed to the fact that the model assumes the plates are flat, ignoring curvature around the circumference. Inclusion of the curvature would significantly stiffen the tyre at low frequencies, thus reducing the response, and increasing the circumferential wavespeed. This idea is supported by the observation that the low-frequency agreement between the measurements and predictions is improved for higher tyre pressures, when the in-plane tension effects will be larger compared with the effects of curvature. Another source of error is associated with the difficulty in accurately estimating the elastic properties of the tyre, which are also likely to be frequency dependent. The method adopted here, described by Hearmon [7], is relatively simplistic, and was used only to ascertain orders of magnitude for the various constants. Finally, the low-frequency tread/sidewall description is simplistic: the constraining effect of the sidewall will be stiffer at lower frequencies than at higher

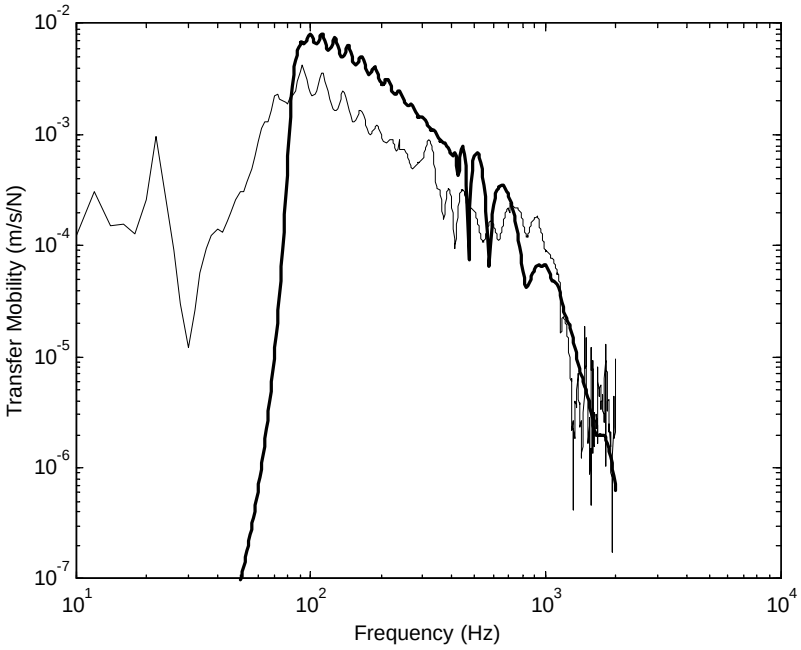

Fig. 11. Measured and predicted transfer response at 2 bar. Response point diametrically opposite the excitation point on the tread; ——; predicted response; —— measured response.

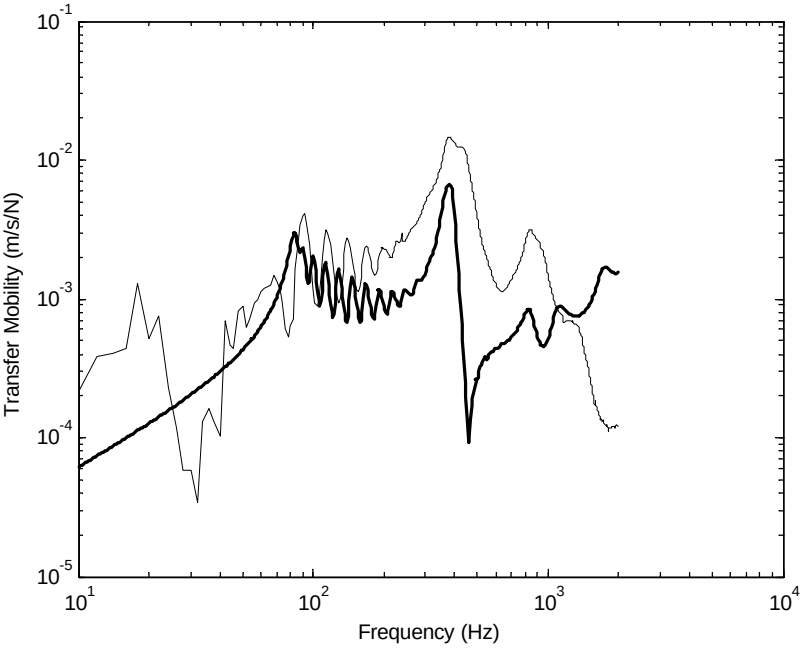

Fig. 12. Measured and predicted transfer response at 2 bar. Response point mid-way along the sidewall, in line with the excitation point; —— predicted response; —— measured response.

frequencies due to shear in the sidewall (e.g. one-quarter of the way around the circumference), rotational constraints, etc. This simplistic model would be expected to be least accurate below the first mode group, as is observed. At such frequencies, however, FE techniques are satisfactory. Furthermore, a resonance of the support structure can be observed around 20 Hz.

Figs. 11 and 12 show the magnitudes of the measured and predicted transfer mobilities at the point on the tread diametrically opposite the excitation point, and mid-way along the sidewall in line with the excitation, respectively. In general, the agreement is good with the observed qualitative features in the measured data being reproduced by the predictions. Comparing the transfer measurements with the corresponding point measurement (Fig. 10c), it can be seen that, as expected, the magnitudes of the transfer responses are less than that of the input mobility. This is due to the waves being significantly attenuated due to damping. This is particularly evident in Fig. 11 for the waves running round the circumference of the tyre. For the sidewall measurement, shown in Fig. 12, unlike the other measurements, the theory tends to underestimate the response. This can be attributed to the relatively crude sidewall model in which the sidewall stiffness is concentrated in the spring at the tread/sidewall junction, rather than distributed along its length.

4. Discussion and conclusions

A simple wave model has been developed to predict the dynamic response of a pneumatic tyre to a line force excitation, aligned circumferentially along the midline of the tyre.

The model predicts that, at low frequencies, below the first resonance, the response is stiffness-like, the stiffness being controlled by the sidewall properties and tension effects resulting from the tyre pressure. The first resonance is associated with "tread bounce", in which the tread moves predominantly as a rigid mass on the sidewall stiffness. Then there follows a set of resonances associated with higher order circumferential modes with the same basic cross-wise motion. At higher frequencies, further groups of circumferential resonances cut on, each with its own characteristic cross-wise response. At high frequencies, the response tends towards that of a point-excited infinite orthotropic plate, limited by the finite length of the excitation line. Changes in internal tyre pressure affect the response at low frequencies as a result of altering the in-plane tensions and the sidewall stiffness. The high-frequency response is largely unaffected by tyre pressure.

Experimental measurements have been made on a treadless tyre in order to confirm the theoretical findings. The results show good agreement for both point and transfer measurements, particularly given the uncertainty over the values for the elastic properties used in the model, with the model accurately reflecting the phenomenological behaviour.

The model is relatively simple, and predicts behaviour in a manner which is easy to interpret. However, it is capable of being extended to be more realistic. Obvious enhancements are the inclusion of the effects of in-plane motion and curvature, improvements to the description of the tread/sidewall junction, and the inclusion of non-uniform properties such as thickness and layer construction. The incorporation of a non-rigid rim into the model is a further possibility. These potential developments are the subject of current and future work.

Acknowledgements

The authors gratefully acknowledge the UK and Korea Science and Technology Fund for their financial support of this work, and Kumho Rubber for providing the tyres and material data.

Appendix A. Determination of sidewall stiffness

In this appendix, an approximate expression is derived for the effective longitudinal stiffness of the sidewall. For modelling purposes, this stiffness is assumed to be discrete and acts at the end of the sidewall which is coupled to the tread, as shown in Fig. 1. In reality, the stiffness is distributed along the length of the sidewall, and arises from a number of possible sources, including axial stretching, bending and shear deformation associated with the sidewall curvature, and pressure/in-plane tension effects. The stiffness due to each of these effects is considered in turn and then combined into a resultant overall stiffness. The sidewall is modelled as a circular arc of radius R, angle $2\theta_0$, with in-plane tension T, along the length of the sidewall, subjected to a force, P, in the x direction as shown in Fig. 13. The aim is to find the total extension, x, of the end B, the stiffness then being $\partial P/\partial x$. It is assumed that the curvature is small.

A.1. Axial stretching

With reference to Fig. 13, the axial force, X_P

$$X_P = P\cos\theta. \tag{A.1}$$

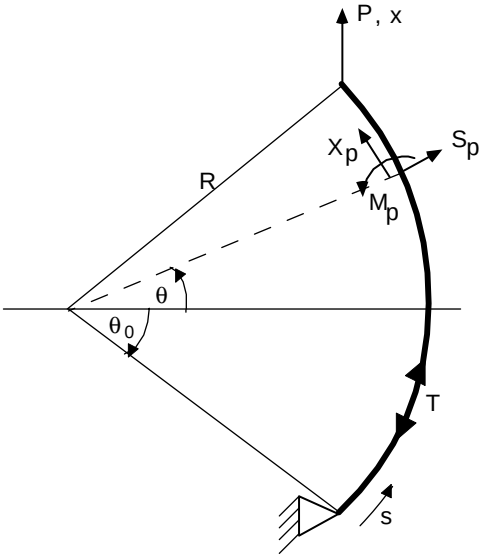

Fig. 13. In-plane sidewall forces and moments.

Neglecting Poisson's ratio effects, using the principle of virtual work [10], the x-wise displacement due to stretching, u_X is given by

$$u_X = \int \frac{\partial X_P}{\partial P} \frac{X_P}{E_x A} \mathrm{d}s, \tag{A.2}$$

where E_x is the x-wise elastic modulus, and A is the cross-sectional area of the sidewall. Integration is performed along the sidewall arc, s, over its entire length.

Substituting for X_P from Eq. (A.1) leads to

$$u_X = \frac{PR}{2E_x A}(2\theta_0 + \sin 2\theta_0). \tag{A.3}$$

A.2. Bending effects

With reference to Fig. 13, the bending moment at any angle, θ, due to an axial force P in the x direction is given by

$$M_P = PR(\cos\theta - \cos\theta_0). \tag{A.4}$$

Using the principle of virtual work, the displacement, u_B, in the x direction due to this force P is given by

$$u_B = \int \frac{\partial M_P}{\partial P} \frac{M_P}{EI} \mathrm{d}s, \tag{A.5}$$

where s is along the arc of the sidewall. Hence

$$u_B = \frac{PR^3}{2EI}(4\theta_0 + 2\theta_0 \cos 2\theta_0 - 3\sin 2\theta_0). \tag{A.6}$$

A.3. Shear effects

With reference to Fig. 13, the shear force, S_P, at any angle θ, due to the applied force P is given by

$$S_P = P\sin\theta. \tag{A.7}$$

Following the same procedure, the displacement produced by shearing action is

$$u_S = \frac{PR}{2GA}(2\theta_0 - \sin 2\theta_0), \tag{A.8}$$

where G is the shear modulus of the sidewall.

A.4. Pressure/in-plane tension effects

This component of the stiffness arises from the fact that, as an axial force, P, is applied to the sidewall, which thus displaces laterally, work is done against the internal pressure; the length of the sidewall remains the same, but its curvature changes.

The tension, T_x, in the sidewall, is related to the axial force applied, P, via

$$P = T_x \cos\theta_0 \tag{A.9}$$

and to the internal pressure, p, by

$$T_x = pR. \tag{A.10}$$

The length, x, in the x direction, of the sidewall is given by

$$x = 2R \sin\theta_0. \tag{A.11}$$

The axial stiffness, K_p, is defined as

$$K_p = \frac{\partial P}{\partial x}. \tag{A.12}$$

which, from Eqs. (A.9)–(A.11) is found to be given by

$$K_p = \frac{p}{2}\frac{(\cos\theta_0 + \theta_0 \sin\theta_0)}{(\sin\theta_0 - \theta_0 \cos\theta_0)}. \tag{A.13}$$

A.5. Combination of effects

Having found the contribution to the sidewall stiffness from the various components above (axial stretching, bending and shear deformation, and pressure/in-plane tension effects), the total sidewall stiffness can now be determined. The displacements due to axial stretching, and bending and shear deformations can be added, so that the component stiffnesses are added in series. The in-plane tension effects effectively constrain the motion, so this stiffness is then added in parallel. This gives the total sidewall stiffness K_s as

$$K_s = K_p + \frac{P}{u_X + u_B + u_S}. \tag{A.14}$$

The two stiffness components are plotted in Fig. 14 as a function of internal tyre pressure for the tyre properties given in Table 1. It is found that the pressure-independent component (the last term in Eq. (A.14)) is dominated by the bending contribution, with the shear deformation and

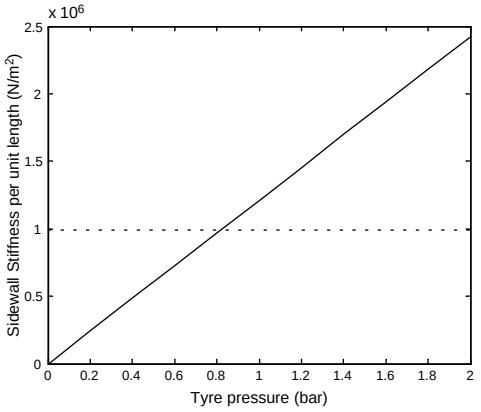

Fig. 14. Sidewall stiffness components: —— pressure/in-plane tension effects; ------ pressure-independent effects.

Table 2
Tread layout and layer properties

Layer[a,b]	Average layer thickness (m)	E_x (N/m^2)	E_y (N/m^2)	G_{xy} (N/m^2)	v_{xy}[c]
Tread	13.0×10^{-3}	4.34×10^6	4.34×10^6	1.45×10^6	0.5
Belt	3.0×10^{-3}	2.07×10^7	1.62×10^8	1.87×10^7	0.0
Ply	1.5×10^{-3}	5.47×10^8	8.07×10^6	1.63×10^7	0.38
Inner	1.5×10^{-3}	4.14×10^6	4.14×10^6	1.38×10^6	0.5

[a] The layers are listed in order from the outer surface of the tyre inwards.
[b] It is assumed that the neutral axis of each section lies along the geometric centre line.
[c] v_{xy} is calculated from $v_{yx} = v_{xy}(E_y/E_x)$.

Table 3
Sidewall layout and layer properties

Layer[a,b]	Average layer thickness (m)	E_x (N/m^2)	E_y (N/m^2)	G_{xy} (N/m^2)	v_{xy}[c]
Sidewall	5.0×10^{-3}	3.93×10^6	3.93×10^6	1.31×10^6	0.5
Ply	1.0×10^{-3}	5.47×10^8	8.07×10^6	1.63×10^7	0.38
Apex	3.0×10^{-3}	1.19×10^7	1.19×10^7	3.95×10^6	0.5
Ply	1.0×10^{-3}	5.47×10^8	8.07×10^6	1.63×10^7	0.38
Inner	1.5×10^{-3}	4.14×10^6	4.14×10^6	1.38×10^6	0.5

[a] The layers are listed in order from the outer surface of the tyre inwards.
[b] It is assumed that the neutral axis of each section lies along the geometric centre line.
[c] v_{xy} is calculated from $v_{yx} = v_{xy}(E_y/E_x)$.

axial stretching effects not being significant. From the figure, it can be seen that, for low tyre pressures, the sidewall stiffness is dominated by bending effects; at high tyre pressures, the stiffness is dominated by pressure/in-plane tension effects. This finding is in accordance with Pinnington [11] who has derived similar expressions for tyre sidewall stiffness.

Appendix B

Material and geometric properties of the tyre are given in Tables 2 and 3.

Appendix C. Estimation of in-plane tensions due to internal pressure

In this appendix, approximate expressions are derived which relate the tensions in the tread and sidewall in the x and y directions to the internal pressure in the tyre. Fig. 15 depicts sectional views of the tyre.

With reference to Fig. 15(a), the x-wise tension in the sidewall can be found by assuming that the sidewall approximates a circular arc of radius R. The tension in the sidewall, T_{sx}, is then related to the internal pressure by

$$T_{sx} \approx pR. \tag{C.1}$$

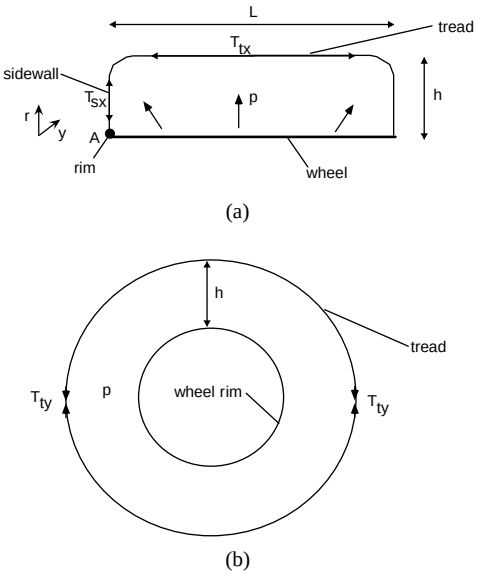

Fig. 15. Tyre sectional views: (a) section through the tyre shown in Fig. 1 and (b) section looking axially through the tyre.

The x-wise tension in the tread, T_{tx}, can be found by taking moments about the rim at A $T_{tx}l_S \approx \int_0^{l_S} pr\,\mathrm{d}r$, where r is measured radially outwards from the wheel rim, giving

$$T_{tx} \approx \frac{pl_S}{2}. \tag{C.2}$$

This ignores any lateral reaction of the rim on the sidewall.

Assuming that most of the circumferential load is taken by the tread, the tread tension in the y direction, T_{ty}, from Fig. 15(b) is given by

$$T_{ty} \approx pl_S. \tag{C.3}$$

Finally, the sidewall tension in the y direction, T_{sy}, is found by assuming that it is approximately equal to the sidewall tension in the x direction, giving

$$T_{sy} \approx pR. \tag{C.4}$$

References

[1] U. Sandberg, Tyre/road noise—myths and realities, Proceedings of the Internoise, 2001, pp. 35–56.
[2] T.L. Richards, Finite element analysis of structural–acoustic coupling in tyres, Journal of Sound Vibration 149 (1991) 235–243.
[3] W. Kropp, Structure-borne sound on a smooth tyre, Applied Acoustics 26 (1989) 181–192.
[4] R.J. Pinnington, A.R. Briscoe, A wave model for a pneumatic tyre belt, Journal of Sound and Vibration 253 (2001) 969–987.
[5] J.S. Bolton, H.J. Song, Y.K. Kim, The wavenumber decomposition approach to the analysis of tire vibration, Proceedings of the Noise-Conference '98, Ypsilanti, MI, Vol. 97, 1998, p. 102.

[6] B.R. Mace, Wave reflection and transmission in beams, Journal of Sound and Vibration 97 (1984) 237–246.
[7] R.F.S. Hearmon, An Introduction to Applied Anisotropic Elasticity, Oxford University Press, Cambridge, England, 1961.
[8] M.A. Heckl, Compendium of Impedance Formulas, Bolt, Beranek and Newman Inc., Cambridge, MA, 1961.
[9] I.J. Busch-Vishniac, Drive point impedance of an infinite orthotropic plate under tension, Journal of the Acoustical Society of America 71 (1982) 368–371.
[10] R.C. Coates, M.G. Coutie, F.K. Kong, Structural Analysis, 3rd Edition, Van Nostrand Reinhold, Wokingham, UK, 1998.
[11] R.J. Pinnington, Radial force transmission to the hub from an unloaded stationary tyre, Journal of Sound and Vibration 253 (2001) 989–1011.